

Article

Pseudo-Planar Organic Heterojunctions by Sequential Printing of Quasi-Miscible Inks

Ana-Gianina Gereanu ¹, Camillo Sartorio ¹ , Aurelio Bonasera ^{1,2} , Giuliana Giuliano ¹, Sebastiano Cataldo ¹, Michelangelo Scopelliti ^{1,2} , Giuseppe Arrabito ^{1,*}  and Bruno Pignataro ^{1,2,*}

¹ Department of Physics and Chemistry-Emilio Segrè, University of Palermo, Viale delle Scienze, bldg. 17, 90128 Palermo, Italy; gianina.gereanu@gmail.com (A.-G.G.); camillo.sartorio@enea.it (C.S.); aurelio.bonasera@unipa.it (A.B.); giuliana.giuliano@unipa.it (G.G.); sebastiano.cataldo@enea.it (S.C.); michelangelo.scopelliti@unipa.it (M.S.)

² INSTM-Palermo Research Unit, Viale delle Scienze, bldg. 17, 90128 Palermo, Italy

* Correspondence: giuseppedomenico.arrabito@unipa.it (G.A.); bruno.pignataro@unipa.it (B.P.)

Abstract: This work deals with the interfacial mixing mechanism of picoliter (pL)-scale droplets produced by sequential inkjet printing of organic-based inks onto ITO/PET surfaces at a moderately high Weber number ($\sim 10^1$). Differently from solution dispensing processes at a high Bond number such as spin coating, the deposition by inkjet printing is strictly controlled by droplet velocity, ink viscosity, and surface tension. In particular, this study considers the interfacial mixing of droplets containing the most investigated donor/acceptor couple for organic solar cells, i.e., poly(3-hexylthiophene) (P3HT) and (6,6)-phenyl-C₆₁-butyric acid methyl ester (PCBM), showing how low-viscosity and low-surface energy inks can be leveraged for the fabrication of an interface suitable for a pseudo-planar heterojunction (pseudo-PHJ) organic solar cell (OSC) that is a convenient alternative to a bulk heterojunction (BHJ) OSC. The resulting thin-film morphology and molecular organization at the P3HT/PCBM interface are investigated, highlighting the roles of dissolution-driven molecular recirculation. This report represents a first step toward the sequential inkjet printing fabrication of pseudo-PHJ OSCs at low consumption of solvents/chemicals.

Keywords: bisolvent droplets; droplet mixing; inkjet printing; pseudo-planar heterojunctions



Citation: Gereanu, A.-G.; Sartorio, C.; Bonasera, A.; Giuliano, G.; Cataldo, S.; Scopelliti, M.; Arrabito, G.; Pignataro, B. Pseudo-Planar Organic Heterojunctions by Sequential Printing of Quasi-Miscible Inks. *Coatings* **2021**, *11*, 586. <https://doi.org/10.3390/coatings11050586>

Academic Editor: Vera Marinova

Received: 22 April 2021

Accepted: 14 May 2021

Published: 17 May 2021

Publisher's Note: MDPI stays neutral with regard to jurisdictional claims in published maps and institutional affiliations.



Copyright: © 2021 by the authors. Licensee MDPI, Basel, Switzerland. This article is an open access article distributed under the terms and conditions of the Creative Commons Attribution (CC BY) license (<https://creativecommons.org/licenses/by/4.0/>).

1. Introduction

The phenomenon of mixing and spreading of droplets is very common because of its great importance for oil pollution on the seawater and rivers [1], and relevant technological applications, such as lab-on-chip devices [2], chemical or biological assays [3], polymer processing [4]. In particular, the manipulation of droplets at the microscale may be carried out by different approaches, such as emulsions [5], microfluidics [6], and printing technologies [7]. Among the latest, inkjet printing (IJP) is one of the most investigated methods, showing remarkable advantages over other droplet deposition approaches, such as spin coating [8], doctor blade [9], and spraying methods [10]. In particular, IJP allows dispensing microsized droplets containing functional inks onto specific substrate locations without the need for photolithographic masks, with volumes ranging from nanoliters to femtoliters [11–13]. Direct fabrication of ultrathin films in selected conditions at solid interfaces is thus achievable [14–16]. Additionally, by ejecting a reproducible quantity of ink without physical contact with the pattern, this technique minimizes any possible contamination on the receiving surfaces [10], paving the way for manufacturing a variety of devices, such as transistors [17,18], nanogenerators [19], fuel cell electrodes [20,21] and solar cells [15,22–26]. Recently, IJP has been leveraged for mixing different chemicals printed as liquid droplets, resulting in the assembly of a number of patterned materials, ranging from polymers to soft biocompatible gels. The possibility to conduce various classes of chemical reactions inside microreactor-like droplets is another fertile area of investigation.

Gold nanoparticles' synthesis [27] or the preparation of alginate-based hydrogels [28] are some examples of established applications, and a few studies started to elucidate the role of solvent evaporation at the droplets' interface, leading to a reduction of the activation energy [29].

Another interesting application of IJP stems from the control on the material interfacial morphological order, which can be leveraged for the fabrication of interfaces featured with tunable interpenetrating domains. A technologically relevant application of these systems can be found in the engineering of planar PHJs for the fabrication of OSCs [30,31]. OSCs are a young member of third-generation photovoltaics (PVs) based on thin films of photoactive organic materials processable at low cost by solution printing methods, becoming key players in all those applications where lightness, flexibility, and cost-effectiveness are welcomed pluses. At the core of this technology, there is the combination of an electron donor (D) and an electron acceptor (A) material. The interface between the D and A layers provides the driving force necessary for the photogenerated excitons to dissociate into free charge carriers upon visible light photons absorption, finally contributing to the passage of electrical current within the device [32]. In this regard, OSCs are generally classified by whether the D and A layers are planar (PHJs) or intermixed (BHJs), respectively. The P3HT/PCBM D/A couple has been the most widely investigated, allowing for power conversion efficiency (PCE) for a P3HT:PCBM BHJ geometry in the interval 3–6%, whereas efficiencies were usually lowered in the case of PHJ P3HT:PCBM architectures, mainly because of the lower D-A interfacial area [33–36]. In order to provide flexibility to OSCs, plastic substrates can be employed instead of glass. In this case, PCE significantly decreases, e.g., for P3HT:PCBM BHJ OSC to 0.08–2.7%, due to the presence of the plastic substrate providing higher surface resistivity of the electrode and lower light transparency [10]. Despite the typically lower PV performances, PHJs can be a valid alternative to the BHJ structure, which usually needs a fine and nontrivial control over nanoscale domains order of the two materials or the employment of suitable interface compatibilizers [32]. As a remarkable advantage, PHJs offer the possibility to employ a sequential printing approach and higher control on the active interface area and on the mixing extent between the two phases [37]. In a previous paper, we have already demonstrated the possibility to increase the PCE of a PHJ OSC significantly [38] by positioning functionalized gold nanoparticle assemblies at the D/A interface. Some recent studies have demonstrated the possibility to realize PHJs by spin coating, in which the partial comixing of the donor and acceptor molecular systems permits to increase donor/acceptor interface and the efficiency of exciton dissociation. These examples are based on sequential spin coating of donor and acceptor solution in quasi-orthogonal solvents to obtain pseudo-PHJ OSCs [37] and, interestingly, nonorthogonal solvents to obtain pseudo-PHJ ternary OSCs [39] and BHJs OSCs [40]. In particular, the pseudo-PHJ architecture seems to provide a valid alternative and effective trade-off between the more common bulk and planar structures, since it features an increased D/A interface area, compared to PHJs, and, at the same time, it ensures continuous percolating pathways for photogenerated charge carriers toward the corresponding electrodes, thereby facilitating charge extraction with respect to BHJ OSCs. Indeed, such a geometry is much closer to the ideal one, which is typically depicted as a bicontinuous interpenetrating network whose interface resembles a herringbone pattern [32]. This concept is clarified and illustrated in Figure 1. Despite the usually lower efficiencies of pseudo-PHJs realized from spin coating using quasi-orthogonal solvents compared to equivalent BHJs, the former architecture is a valid alternative to the latter since it combines all the aforementioned advantages related to the PHJ processing (sequential printing approach, higher control of the interfacial area, etc.), resulting in a higher control over the charge separation and extraction. Another advantage of the pseudo-PHJ geometry is constituted by the enhanced device stability, compared to BHJ OSCs, which typically suffer from poor stability of the interfacial morphology in the long term due to phase separation mechanisms [32].

In all the aforementioned works devoted to pseudo-PHJs, the effects of interfacial mixing between D and A are described as the result of the partial (or complete) mixing of the sequentially deposited thin films during the deposition process. However, the spin coating technique used in those reports is limited by the fast solvent evaporation during the ink deposition, limiting the possibility to control the mixing and involving a high consumption of materials. To this aim, the employ of additive manufacturing techniques such as IJP could add further control of the intermixing phenomena between sequentially printed layers. However, to our knowledge, the role of mixing and molecular recirculation in printed droplets for the fabrication of pseudo-PHJs has not been investigated yet.

To bridge such a knowledge gap, this research report presents the IJP-based fabrication of a pseudo-planar interface via sequential inkjet printing of quasi-miscible droplets for integration into pseudo-PHJ OSCs, investigating the most relevant physicochemical mixing phenomena. By reaching a good control over droplet deposition, ink viscosity, and surface tension, it is possible to bring to a facile, controllable interface remixing. In particular, this study establishes a low-cost approach to fabricate P3HT:PCBM pseudo-PHJ OSCs in ambient conditions onto plastic substrates, i.e., indium tin oxide coated polyethylene terephthalate film (ITO–PET). Plastics supports have been chosen to investigate OSCs whose fabrication could be readily scaled up to industrial production level; the reason behind their success is related to their distinctive features such as lightweight [41], flexibility/stretchability [42], and cost-effectiveness [43], all together shortening the stretch between research prototype devices and large-scale industrial manufacturing. For instance, it is more than 20 years that flexible OSCs have been successfully integrated into clothing [44,45]. A single-pulse waveform signal is employed to print satellites-free droplets containing P3HT and PCBM at reasonable concentrations to produce thin films characterized by uniform morphology and reduced ink consumption, highlighting the possibility to leverage bisolvent droplets for controlling the interfacial mixing process and the Marangoni flows.

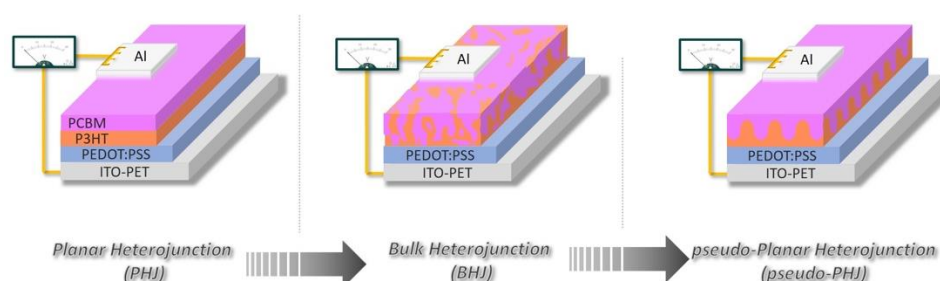


Figure 1. Schematics of the PHJ, BHJ, and pseudo-PHJ architectures for OSCs.

2. Materials and Methods

2.1. Chemicals

The solvents employed in this study were purchased at Merck/Sigma-Aldrich (Munich, Germany) and used without further purification. The following chemicals were also purchased and used without any further purification, if not specifically detailed in the next sections. Poly(3-hexylthiophene-2,5-diyl) (P3HT, regioregular, 91–94%, electronic grade, average M_n 50–70 kDa) was purchased at Rieke Metals, Inc. (Lincoln, NE, USA); (6,6)-phenyl- C_{61} -butyric acid methyl ester (PCBM, 99.5%) was purchased at Solenne BV (Groningen, The Netherlands); glycerol (ACS reagent, $\geq 99.5\%$) and poly(ethylenedioxythiophene):poly(styrenesulfonate) (PEDOT:PSS) dispersion in water (1.3 wt.%, conductive grade) was purchased at Merck/Sigma-Aldrich. Indium tin oxide (ITO) glass substrates (surface resistivity $10 \Omega \cdot \text{sq}^{-1}$) were purchased at Visiontek Systems Ltd. (Chester, UK); ITO-coated polyethylene terephthalate (ITO–PET) substrates (surface resistivity $60 \Omega \cdot \text{sq}^{-1}$, ITO layer average thickness $\sim 1100 \text{ \AA}$) were purchased at Merck/Sigma-Aldrich.

2.2. Inks Preparation

The PEDOT:PSS ink was prepared by adding glycerol (final concentration: 20 vol.%) to the PEDOT:PSS aqueous solution provided by the producer (final glycerol concentration: 20 vol.%). The mixture was stirred for 30 min and filtered through 0.45 μm hydrophilic PVDF filters. P3HT was dissolved in anhydrous chlorobenzene (99%) in order to prepare the ink solution (10 $\text{mg}\cdot\text{mL}^{-1}$), whereas PCBM dissolved in anhydrous dichloromethane (99%) in order to prepare the ink solution (5 $\text{mg}\cdot\text{mL}^{-1}$). Inks were stirred for about 30 min and subsequently filtered through a 0.45 μm PVDF filter. In the case of PHJs device, P3HT and PCBM were sequentially deposited on the PEDOT:PSS film. In the case of BHJs device, P3HT and PCBM (1:0.8 wt./wt.) were dissolved in anhydrous chlorobenzene (99%) to prepare the final ink (9 $\text{mg}\cdot\text{mL}^{-1}$) and printed onto the PEDOT:PSS film.

2.3. ITO/Glass and ITO/PET Substrate Preparation

The substrates for OSCs were sequentially cleaned by sonication in methanol, acetone, and isopropanol for 20 min each, followed by cleaning in a ProCleaner Plus UV ozone cleaner (Bioforce Nanosciences, Salt Lake, UT, USA) for 60 min.

2.4. Fabrication of PHJs and BHJs by Inkjet Printing

Picoliter-scale droplets of polymer inks were dispensed by using a DMP-2800 Dimatix Materials Printer (FUJIFILM Dimatix, Inc., Santa Clara, CA, USA) at 40% relative humidity. This instrument was equipped with user fillable piezo-driven inkjet print cartridges, each with 16 nozzles 254 μm spaced 21.5 μm (10 pL) in diameter. Droplet formation at the nozzles was executed by suitable waveforms (i.e., the voltage vs. time signal given as input to the piezoelectric actuator). In the case of PEDOT:PSS ink, which has favorable physicochemical properties (viscosity and surface tension), the conventional double pulse waveform was employed, (frequency: 5 kHz, jetting voltage: 30 V), drop spacing (35–60 μm), with the substrate temperature kept at 60 $^{\circ}\text{C}$. The PEDOT:PSS ink was printed on the substrate and dried at 100 $^{\circ}\text{C}$ (1 h) on a hot plate under air to form a thin film serving as the hole transport layer (HTL) in the final solar cell device. As a comparison, reference samples were prepared by spin coating PEDOT:PSS films at 4000 rpm and again dried at 100 $^{\circ}\text{C}$ on a hot plate under air.

In the case of P3HT and PCBM inks, a single pulse waveform was employed in order to avoid satellite production. The P3HT ink was printed on the PEDOT:PSS film by employing a single pulse waveform (frequency: 3 kHz, jetting voltage in the range 26–27 V) and a constant drop spacing (55 μm). The PCBM ink was printed on the P3HT/PEDOT:PSS film by employing a single pulse waveform (frequency: 2 kHz, jetting voltage: 23 V) and a constant drop spacing (55 μm). Similar to P3HT ink, the P3HT:PCBM ink was printed by employing a single pulse waveform (frequency: 2.5 kHz, jetting voltage in the range 26–27 V) and a constant drop spacing (55 μm). In all the experiments, the size of the patterns was kept constant to 20 \times 20 mm^2 . After deposition of the active films, all the samples were transferred in a MBraun gloveboxes system (MBraun Intergas-Systeme GmbH, Garching, Germany) filled with N_2 (<0.1 ppm in O_2 and H_2O), in order to thermally evaporate 100 nm-thick Al layer at a deposition rate of about 1 nm/s as the metal top electrode to complete the devices. The active area of each electrode was equal to approx. 0.13 cm^2 .

2.5. Spectroscopic and Morphological Characterization

A Varian Cary 5 spectrophotometer (Varian Inc. now Agilent Technologies Inc., Santa Clara, CA, USA) and 2 mm optical path quartz cells were used for UV–Visible optical absorption.

2.6. Atomic Force Microscopy (AFM)

AFM imaging was performed by a Multimode/Nanoscope V (Bruker, Billerica, MA, USA). The images were acquired by using commercially available etched-silicon probes

(RTESP type, Bruker) and collecting 512×512 pixels per image by maintaining the scan rate at about 1 line/s. The AFM images were elaborated and by the software Gwyddion vers. 2.55 [46]. Flattening and smoothing algorithms were applied to the selected images prior to evaluating the surface roughness (the analysis was extended to an area of $5 \times 5 \mu\text{m}^2$).

2.7. X-ray Photoelectron Spectroscopy (XPS)

XPS spectra were acquired with a ULVAC–PHI PHI 5000 VersaProbe II scanning microprobe (Chigasaki, Japan) using monochromatic Al $K\alpha$ radiation ($h\nu = 1486.6$ eV), 200 μm spot, 50 W power, 15 kV acceleration, and 45° takeoff angle. Profiles were obtained via Ar^+ sputtering (acceleration 1 kV, rastering surface $2 \times 2 \text{mm}^2$), collecting a full spectrum every 12 s (0.2 min) of sputtering. All spectra were collected using a dual neutralization system (both e^- and Ar^+).

2.8. Electrical Measurements

Photovoltaic devices were characterized by using a halogen lamp as the illumination source, having an irradiance power of $100 \text{mW}\cdot\text{cm}^{-2}$ (1 sun). For calibration, a commercial Si reference cell was used (model 15151, Abet Technologies, Milford, CT, USA). Current-voltage curves were acquired by using a Keithley 2400 source meter (Tektronix, Inc., Beaverton, OR, USA). All the measurements were performed in a glovebox system under an N_2 atmosphere (<0.1 ppm of O_2 and H_2O) at room temperature.

3. Results

3.1. Inkjet Printing P3HT:PCBM Inks

At first, it was developed a method to IJP P3HT or PCBM inks, prepared by dissolving P3HT ($10 \text{mg}\cdot\text{mL}^{-1}$) in chlorobenzene, and PCBM ($5 \text{mg}\cdot\text{mL}^{-1}$) in a 1:1 mixture of chlorobenzene and dichloromethane, respectively. The choice of the solvents in this study is somehow driven by the solubility of the materials, and halogenated aromatics are quite common solvents in printing technology [31], as reported in Table S1. Initially, the Ohnesorge number (Oh) of these fluids was evaluated to verify their suitability for IJP. This number is defined as $\text{Oh} = \mu / \sqrt{\rho\sigma L}$, where ρ is the liquid density, σ is the surface tension, L is the characteristic length scale (i.e., drop diameter), and μ is the dynamic viscosity of the fluid. By substituting the estimated values for our ink ($\rho \approx 10^3 \text{kg}\cdot\text{m}^{-3}$, $\sigma \approx 72 \times 10^{-3} \text{kg}\cdot\text{m}^{-3}$, $L \approx 20 \times 10^{-6} \text{m}$, $\mu \approx 1 \text{mPa}\cdot\text{s}$), it is possible to evaluate an Oh number of about 25. The ink jettability was then predicted using the Fromm number (Z), which is the inverse of the Ohnesorge number, $Z = 1/\text{Oh}$. For a fluid to be printable and to avoid the formation of satellites, the Z number has to be in the range comprised between 1 and 10 [9]. The calculated value for the above-considered inks ($Z = 26$) is outside the range of ideal inkjet fluids ($1 < Z < 10$), but rather it can lead to the production of satellites (as reported in the Supplementary Materials, Figure S1). In order to avoid this, a single pulse voltage waveform was employed, as reported in Figure 2a. This waveform is specifically suited for printing low viscosity inks [13] by reducing the length of the droplet thread after pinching off at nozzle, finally avoiding multiple breakups and satellite formation. This is accomplished by increasing the phase of voltage decrease (the t_F reported in Figure, which lasts about 17 μs) with respect to the conventional double pulse waveform of about 5 μs (see Supplementary Materials), with the aim to maximize the negative pressure that pulls back the liquid thread toward the nozzle. Figure 2b reports the droplet formation following the optimized conditions (jetting voltage equal to 27 V). As it is possible to observe, the satellite droplet rapidly recoils with the primary droplet after about 100 μs . The velocity of the resulting droplet is about $8 \pm 1 \text{m}\cdot\text{s}^{-1}$. Given that the diameter of P3HT droplets on PEDOT:PSS is about 60 μm , a droplet spacing of 55 μm was found to allow for the optimal droplet coalescence in printed lines having straight contour without line bulging [15]. PCBM IJP was accomplished by using the previously optimized waveform. However, the choice of the solvent for PCBM plays a fundamental role. Accordingly, PCBM solutions are usually prepared in dichloromethane, an orthogonal solvent to chlorobenzene when

preparing PHJs by spin coating [38]. However, since dichloromethane is a low-boiling point solvent, droplet formation was not possible due to the rapid ink evaporation at nozzles and finally clogging. Similar results were obtained by printing PCBM in isopropanol, which has a higher boiling point (82 °C).

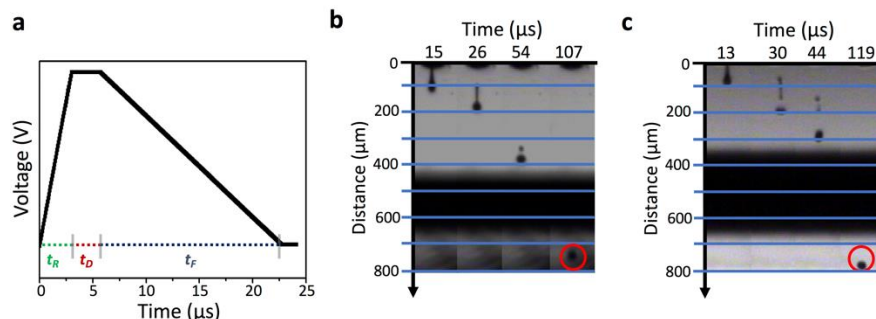


Figure 2. Inkjet printing P3HT and PCBM inks: (a) single-pulse waveform signal, composed of three phases of rise (t_R), dwell (t_D), and fall (t_F); stroboscopic images showing droplet formation and satellite recoil at various acquisition times for P3HT ink (b) and PCBM ink (c) finally permitting us to print an almost spherical droplet in both cases (see the droplet within the red circle).

Differently, it was possible to successfully produce PCBM ($5 \text{ mg}\cdot\text{mL}^{-1}$) in an ink prepared in a 1:1 mixture in dichloromethane and chlorobenzene given the lower vapor pressure of solvents mixture in comparison to pure dichloromethane [47], avoiding nozzles clogging. This was possible since chlorobenzene was added at 50 vol.% permits a twofold reduction of the vapor pressure [48], improving the reproducibility of the IJP process. PCBM droplets were printed in similar conditions to P3HT (see the Derby plot reported in Figure S1 in the Supplementary Materials) with the only difference to maintain a slightly lower jetting frequency (2 kHz instead of 3 kHz) and lower jetting voltages (22 V vs. 26 V). The stroboscopic characterization of the corresponding printed droplet (produced at the jetting voltage equal to 22 V) is reported in Figure 2c. The speed of the droplet is equal to $7 \pm 1 \text{ m}\cdot\text{s}^{-1}$, still resulting optimal in terms of trajectory accuracy [49]. The choice of these experimental conditions was made to cope with the lower viscosity of the resulting ink due to the presence of dichloromethane, which has lower viscosity in comparison to chlorobenzene, respectively, $0.41 \text{ mPa}\cdot\text{s}$ versus $0.75 \text{ mPa}\cdot\text{s}$. Different from P3HT or PCBM printing, PEDOT:PSS IJP was carried out by employing a conventional double pulse waveform, given the higher viscosity of the ink. This leads to the formation of liquid threads with lengths higher than $400 \mu\text{m}$. The droplet resulted stable against the formation of satellites though, as an effect of glycerol that permits us to increase its viscosity and the capillary instability induced breakups. The resulting droplets were typically printed at 23 V, resulting in a speed of about $13 \pm 3 \text{ m}\cdot\text{s}^{-1}$, and with a droplet-to-droplet spacing equal to $55 \mu\text{m}$ (see Figure S2 in the Supplementary Materials).

3.2. Morphological and Chemical Characterization of the Printed P3HT/PCBM Interface

After having optimized the IJP processes, the study proceeded with an in-depth morphological and chemical characterization of the as-deposited P3HT and PCBM layers and their corresponding interface. In particular, Figure 3 reports on the AFM investigation of the IJP pattern of P3HT droplets onto PEDOT:PSS printed film. Accordingly, given that the surface energy of the hydrophobic P3HT layer is significantly lower (about $25 \text{ mN}\cdot\text{m}^{-1}$) than PEDOT:PSS (about $70 \text{ mN}\cdot\text{m}^{-1}$), the former will homogeneously cover the last layer without dewetting phenomena. The lateral phase separation of the P3HT film was investigated by AFM, revealing a very smooth surface morphology, obtaining an average roughness value equal to 1.1 and 1.4 nm, for films prepared by inkjetting at 27 V and 40 V, respectively. Figure S3 reports on the P3HT film printed at 40 V. Interestingly, at the border of the printed pattern, it is possible to observe an accumulation of P3HT, likely resulting from the higher solvent evaporation flux with respect to the center of the droplet.

The printed PCBM film can be easily distinguished from the underlying printed P3HT film. The PCBM molecules are able to produce a well-defined and compact film at the center of the printed droplet, with a roughness of about 1.3 nm. Differently, at the droplet border, it is possible to observe the formation of disconnected PCBM aggregates. These are characterized by lateral sizes and heights in the range of 200–400 nm and 10–20 nm, respectively, leading to the roughness of about 11–12 nm (see Figure 3). By increasing the PCBM inkjetting voltages up to 40 V, the lateral size of the PCBM aggregates increased (Figure S4), eventually leading to continuous aggregated with heights of about 20–30 nm, being the average surface roughness equal to 11 nm.

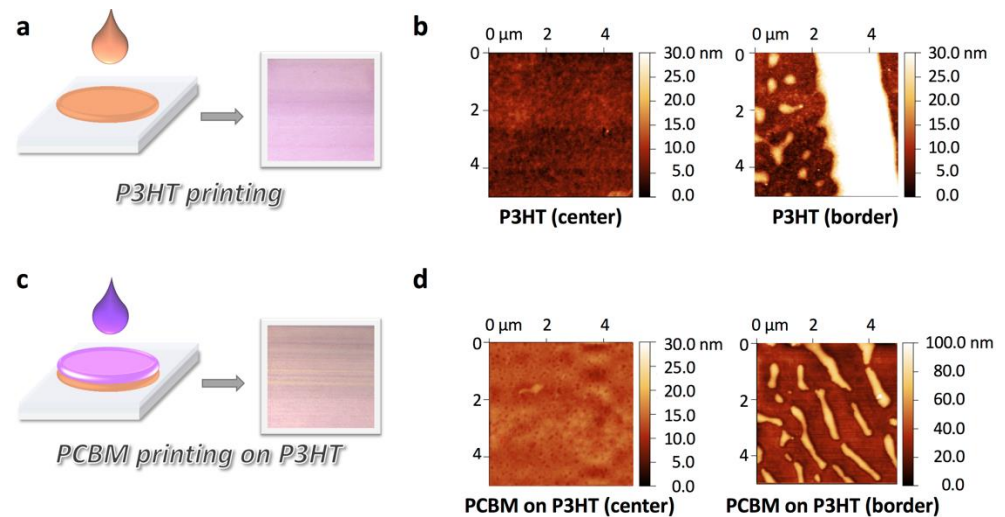


Figure 3. Optical and AFM characterization of the sequentially inkjet-printed P3HT:PCBM patterns: (a) P3HT droplet deposition and optical characterization of the resulting printed P3HT layer ($20 \times 20 \text{ mm}^2$); (b) AFM characterization of the printed film within the center of the P3HT droplet (image at the left) and the border of a single droplet (image at the right); (c) PCBM droplet deposition on the top of the previously printed P3HT layer, leading to a P3HT:PCBM layer; (d) AFM characterization of the printed film at the center (image at the left) and at the border (image at the right) of the printed PCBM droplet.

The fluorescence characterization of the printed PHJs demonstrated the occurrence of quenching of the typical P3HT fluorescence emission band at about 655 nm when the PCBM layer is printed on top of P3HT (see Figure 4). This almost total quenching is due to the electron transfer process occurring from the excited P3HT lowest unoccupied molecular orbital (LUMO) to the PCBM LUMO after light absorption, and it is indicative of an effective D/A interface contact.

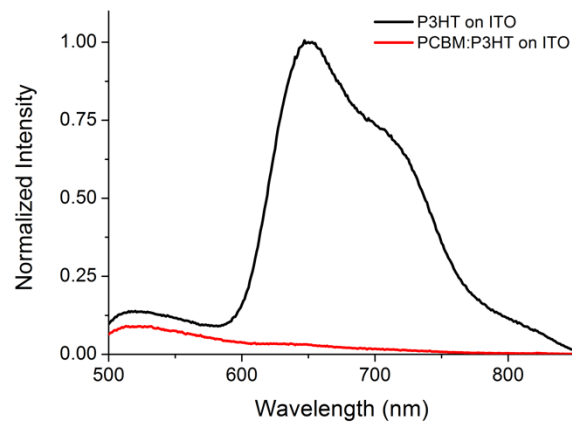


Figure 4. Fluorescence spectra of the P3HT printed film (black line) and of the P3HT:PCBM film (red line), showing the almost complete fluorescence quenching.

In order to investigate possible intermixing effects, an XPS depth profile (see Figure 5) was acquired on a printed P3HT:PCBM PHJs. Notably, the rather mild sputtering conditions (1 kV) were chosen to reduce the damage to the underlying printed structures. Indeed, these experimental conditions for the cross-section investigation of the printed films were optimized in previous articles from our group [38,50], resulting in suitable conditions for organic-based thin films obtained by solution-dispensing methodologies. In those reports, we proved that thin films produced by spin coating using orthogonal solvents showed no significant intermixing between the P3HT and PCBM layers, thus ruling out any effect due to the high energy transmitted by the Ar^+ ions toward interlayer mixing.

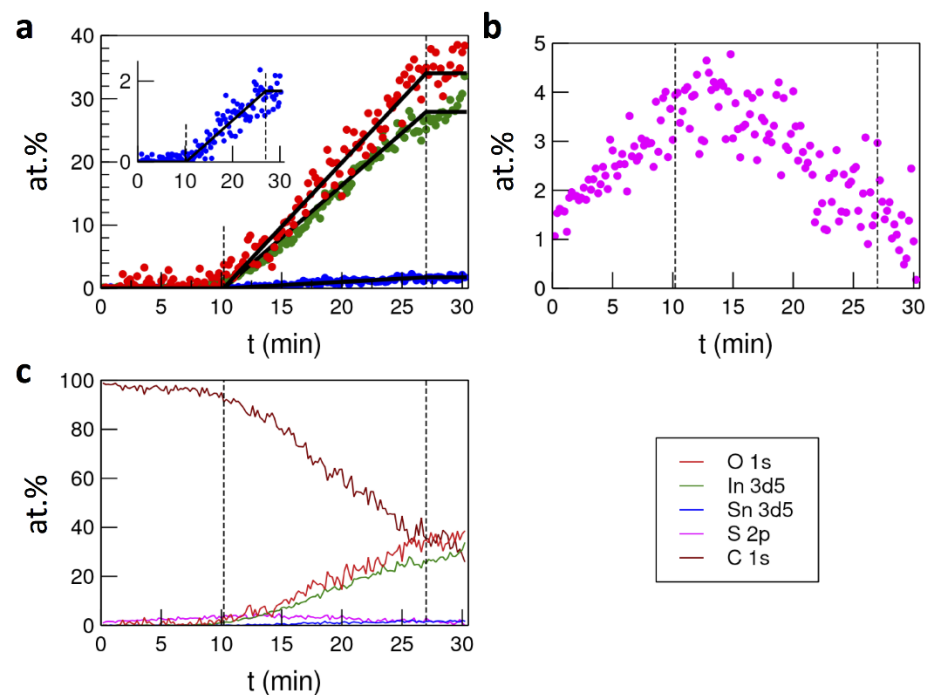


Figure 5. XPS depth profile characterization of (a) the ITO layer, (b) the relative S abundance, and (c) the overall elemental depth profile distribution from the printed layers onto ITO. The elemental depth profiles (reported as dots or lines) are obtained by analyzing the following species: O 1s (red), In 3d5 (green), Sn 3d5 (blue), S 2p (magenta), C 1s (brown).

In a perfectly stacked multilayer system, one would expect a succession of slopes and/or plateaus corresponding to the relative abundance of the observed elements, with the plateau values in atomic percentages (at.%), indicating the composition for the observed

material, and every slope indicating a transition between different layers. This is evident in Figure 5a, where the increase of In, Sn, and O (starting at 10.2 min) marks the appearance of the ITO layer. The clearing of the overlying films is reached at 27.0 min (clearing window: 16.8 min). In a previous study from our group [50], we reported how the slope time is related to the sampling depth of the XPS technique; therefore, it is clearly visible how the sum of the layers over the ITO has a total thickness lower than 7 nm (assuming a sampling depth of $\lambda \sin \theta$, with λ indicating the inelastic mean free path in the material, ca. 10 nm for Al K α , and θ indicating the takeoff angle). In this case, it is neither possible to have a clear picture of the layer thickness, due to the fact that it is not conceivable to reach the expected values of elements at.% because of geometrical considerations, nor it is possible to convert between time (min) and space (nm) scales. Nonetheless, besides the quantitative analysis inadequacy, the qualitative analysis (i.e., the layer stacking) is still possible, given that every change in the slope should mark a net change in the composition for a given element. Looking at Figure 5b, showing the S relative abundance (S 2p region) due to the PEDOT:PSS and P3HT systems, it is evident how such net separations do not exist. These fluctuations may only be justified by a mixing of different layers, creating local gradients not relatable to the expected stratification. Moreover, it is possible to observe how S is still present after the complete ablation of the layers above the ITO. The fact that both S and C maintain a relative abundance higher than 0 inside the ITO layer (Figure 5c) might likely suggest that the printed material has spilled inside the ITO; it is unclear if such a spilling is caused by the printing process or if it happened because of the commonly occurring cracks onto the ITO surface.

3.3. Electrical Characterization of the Photovoltaic Devices

Table 1 reports on the photovoltaic parameters obtained for the three different OSC systems fabricated in this work (see the Experimental Section), which differ in the number and type of components deposited by IJP (the P3HT:PCBM PHJ only, the P3HT:PCBM BHJ only, and both the PEDOT:PSS HTL and the P3HT:PCBM BHJ, respectively). The OSC performance reproducibility of the printed devices was further tested by repeating the electrical characterization in three different experiments; the mean values are reported in Table S2. Interestingly, the photovoltaic parameters corresponding to the best performing PHJ deposited onto ITO/PET under air conditions ($J_{sc} = 0.82 \text{ mA}\cdot\text{cm}^{-2}$; $V_{oc} = 0.31 \text{ V}$, FF = 0.30; PCE = 0.08%) are quite comparable to those obtained in our previous reference study [38] conducted in glove box under inert nitrogen atmosphere by employing spin coating ($I_{sc} = 0.82 \text{ mA}\cdot\text{cm}^{-2}$; $V_{oc} = 0.48 \text{ V}$; FF = 0.38; PCE = 0.15%). In particular, the best PHJ device fabricated in this study exhibited the same value of J_{sc} as that yielded by the top device reported in the previous work, as well as quite comparable FF. This suggests that the present approach, which involves a substantial interfacial mixing at the P3HT:PCBM junction, is effective in producing relatively pseudo-PHJs OSCs at good performance without the need for inert atmosphere processing and by using low-cost IJP technique (with all its aforementioned advantages over spin coating in terms of morphology control and materials waste).

Table 1. Summary of OSC performances (short-circuit current, J_{sc} ; open-circuit voltage, V_{oc} ; fill factor, FF; power conversion efficiency, PCE) for solar cells having PET/ITO/PEDOT:PSS/P3HT:PCBM (PHJ or BHJ)/Al structure and differing from each other in the number and type of components deposited by IJP. In particular, the investigated printed components are the P3HT:PCBM PHJ, the P3HT:PCBM BHJ, and the HTL+BHJ in which both the PEDOT:PSS HTL and the P3HT:PCBM BHJ are realized by IJP.

Inkjet-Printed Component	J_{sc} ($\text{mA}\cdot\text{cm}^{-2}$)	V_{oc} (V)	FF -	PCE (%)
P3HT:PCBM PHJ	0.82	0.31	0.30	0.08
P3HT:PCBM BHJ	2.99	0.60	0.34	0.61
PEDOT:PSS HTL+ P3HT:PCBM BHJ	4.60	0.53	0.27	0.67

In addition to PHJs, BHJ OSCs were also fabricated and characterized for comparison purposes (see Table 1). As expected, all the photovoltaic parameters obtained for the BHJ OSCs are significantly higher than those of the PHJ ones fabricated in our study. This can be ascribed to the substantial gain in terms of the interfacial area provided by the BHJ structure. Importantly, the photovoltaic parameters of our best performance BHJ devices are even higher than those reported for other devices produced by spin coating onto glass supports under similar conditions [51]. This demonstrates that, despite the typical disadvantages of employing plastic substrates in terms of higher electrical resistance and lower optical transmittance, it is possible to obtain flexible BHJ OSCs with higher PV performances than those of analog devices deposited onto glass supports through careful optimization of the printing conditions. Curiously, the device in which both the PEDOT:PSS HTL and the P3HT:PCBM BHJ were deposited by IJP showed a slightly higher PCE compared to that of the other BHJ solar cell. This improvement cannot be simply ascribed to better morphological/electrical properties of the PEDOT:PSS film produced by IJP, since this would correspond to a more efficient hole extraction at the anode and hence to a higher FF value, which is not observed (the FF decreases from 0.34 to 0.27). On the other hand, it can be noted from Table 1 that the higher PCE value is mainly due to a substantial increase in the J_{sc} ($4.60 \text{ mA}\cdot\text{cm}^{-2}$ against $2.99 \text{ mA}\cdot\text{cm}^{-2}$), which rather suggests a better morphology of the BHJ active layer on top of the inkjet-printed PEDOT:PSS layer, leading to a more efficient charge carrier generation.

Printing techniques enable the large-scale realization of OSCs, permitting the reduction of material consumption with respect to spin coating [30]. In turn, the formulation of printable inks for the fabrication of OSCs devices (especially PHJs) becomes necessary, allowing for PCEs at least comparable to those from devices obtained from the spin coating. To this aim, the quasi-miscible inks formulation investigated in this study exploits intermixing processes occurring between the printed layers, permitting the increase of the D/A interface area and resulting in PCEs similar to those obtained from PHJs from our previous reference study [38], realized by spin coating in glove boxes. Therefore, the here-described intermixing phenomena between sequentially printed layers could be a first step toward the fabrication of a novel class of printed pseudo-PHJs. It is worth noting that the performances obtained for the pseudo-PHJ OSCs are still lower than those of the reference BHJ counterparts, as typically observed in the literature reports where spin-coating deposition is employed [37,39]. However, we believe that, differently from spin coating, the proposed printing approach can lead to more stable, reproducible, and easily scalable devices with possibly higher appeal in the perspective of a future large-scale OSC commercialization, enabling a sequential printing of the constituent materials and a consequent higher control of the interfacial properties and showing much room for improvement.

Taken together, these data suggest that, under our experimental conditions, the proposed ink formulations and deposition methods are able to produce P3HT:PCBM pseudo-PHJs and BHJs with remarkable PV performances. In particular, the proposed sequential IJP deposition of quasi-miscible inks can be exploited to obtain P3HT:PCBM pseudo-

PHJs with good control on the nanomorphology, resulting in an efficient charge carrier generation/extraction in the corresponding OSC devices as a result of the controlled inter-diffusion of the PCBM nanoparticles into the preprinted P3HT film, as will be discussed in detail below. Through this method, it is possible to achieve good performances by using low-cost IJP technique, under air conditions (without the need for expensive inert atmosphere equipment) and onto plastic substrates (making these systems suitable also for integration into modern flexible optoelectronic devices).

4. Discussion

Intermixing processes in the solutions employed for the fabrication of solar cells have been investigated in many reports that employ quasi-orthogonal [37] or nonorthogonal [39,40] solvents. These studies focused on spin coating processed devices, and in particular, on the P3HT:PCBM PHJs and BHJs based OSCs [52,53]. If one considers the typical process of droplet dispensing by spin coating, this typically involves an initial stage lasting a few milliseconds in which the droplet deposited on the rotating spinning substrate is thinned mainly due to the radial convection outflow and a second stage in which the solvent mass transfer to vapor leads to evaporation and finally thin film formation [8]. A totally different scenario occurs in the case of the formation of printed droplets. Once the droplet is formed, it reaches the substrate in the timescale of a few milliseconds. Following the model of Hu [54], the droplet spreads on the surface and the solvent evaporation takes place in time scales of microseconds to seconds, being dependent on many factors, such as wettability, relative humidity, and droplet radius. It is possible to estimate the evaporation time of a picoliter scale printed droplet containing polymers dissolved in chlorobenzene to be of the order of 10^{-5} – 10^{-4} s, following the constant contact-area evaporation mode, in which the contact angle decreases with time maintaining a constant contact area with the receiving substrate [55]. The mixing between the jetted films can be then estimated following the Noyes–Whitney model [56] as follows:

$$\frac{dC}{dt} = \frac{DS_w}{Vh} (C_s - C) \quad (1)$$

where C , C_s , S_w , D , V , and h indicate the concentration of the dissolved system at a time t , the solubility concentration of the substance, the surface area of exposed solid, the diffusion coefficient of the substance, the volume of solution, and the thickness of the diffusion layer, respectively. An integrated form of this equation can be useful to estimate the concentration of the dissolved material at a given time t under the terms of $C = 0$ at $t = 0$.

$$C(t) = C_s \left\{ 1 - e^{-\frac{DS_w}{Vh} t} \right\} \quad (2)$$

Importantly, PCBM can in principle diffuse at a higher extent with respect to the P3HT molecules in the printed droplet before evaporation occurs, given its lower molecular weight and hence higher diffusion coefficient with respect to P3HT. In fact, considering its molecular weight, PCBM can reach a diffusion coefficient of 10^{-5} $\text{cm}^2 \cdot \text{s}^{-1}$ when dissolved in a solvent and up to 10^{-9} $\text{cm}^2 \cdot \text{s}^{-1}$ when dried with P3HT [57], diffusing in the deposited droplet before evaporation, ultimately remixing the P3HT/PCBM interface. By knowing the solubility of P3HT and PCBM in the solvents [58], this model predicts that the PCBM printed film can well mix with the underlying P3HT, given that in 10^{-6} s, the PCBM molecules can well diffuse at nanometer scale distances. The subsequent annealing process further facilitates the PCBM mixing in P3HT [57]. The XPS depth profiles of this study fully confirm the intermixing of the printed layers.

As far as the gravitational forces are concerned, an important difference arises between the spin coating and IJP. Such effects are quantified by the Bond number (B_0) defined as $\rho g l^2 / \sigma$, where ρ is the density, g is the gravity acceleration, l is the characteristic length, and σ is the surface tension. In contrast to the droplets at the macroscale used for spin coating, which have a Bond number approaching 1, the microscale droplets are characterized by

a significantly lower Bond number (10^{-4} – 10^{-5}); hence, the distribution of the printed molecules on the solid surface is significantly affected by surface tension gradients due to both variations in temperature and liquid composition. In this scenario, the solute is generally transported from the center of the droplet to the edge, potentially forming a ring-like profile [59], which could affect the uniformity of the polymeric film, especially if stacked layers are printed one on the top of the other. Importantly, inkjetted droplet evaporation on the substrate is crucially important for avoiding the “coffee-ring” effects, permitting us to achieve an almost-uniform film coverage on the substrate. This unwanted effect can be solved by facilitating solvent evaporation, in order for it to be faster than the capillary flows to the droplet border. Accordingly, the bisolvent mixture used for printing PCBM (dichloromethane:chlorobenzene at 1:1 ratio) allows reducing the volatility of the printable ink with respect to the conventional dichloromethane-based ink for orthogonal solvent, to avoid nozzle clogging. Along with less volatility, chlorobenzene has a higher surface tension with respect to dichloromethane, being, respectively, 33.6 and 26.5 mN·m⁻¹ in ambient conditions. The surface tension of the mixture can be estimated considering the models presented by Eales et al. [60], according to which the resulting value of the mixture is reduced in comparison to the simple linear relation of the constituents, following the theoretical approach initially described by Suri and Ramakrishna [61] as follows:

$$\gamma = \gamma_1^* x_1 + \gamma_2^* (1 - x_1) \pm \frac{A}{2RT} (\gamma_1^* - \gamma_2^*) x_1 (1 - x_1) \quad (3)$$

where γ_1^* and x_1 are the surface tension and the liquid-phase mole fraction of component 1 (chlorobenzene), γ_2^* and x_2 are the surface tension and the liquid-phase mole fraction of component 2 (dichloromethane), A (cm²·mol⁻¹) is the molecular surface occupancy, R is the universal gas constant, and T is the absolute temperature. The gradients in surface tension lead to the formation of instabilities within the droplet, resulting in Marangoni flows. Eales et al. [60] have modeled such instabilities for IJP microdroplets, employing a linear stability analysis. In doing so, they identified that if the more volatile liquid has a lower surface than that of the less volatile liquid, the Marangoni flows would occur at the border of the droplet, whereas in the opposite case (more volatile liquid has a higher surface than that of the less volatile liquid), the instability would occur at the center of the droplet. Our results are well in accord with the first scenario, being chlorobenzene less volatile and possessing higher surface tension and hence, resulting in instabilities formed just at the droplet edge. Consequently, the Marangoni stresses on the accumulated PCBM at the droplet border trigger the formation of fingering instabilities at the droplet contact line, as shown by the AFM characterization. Interestingly, the sizes of such fingers are increased by raising the jetting voltage used for printing the PCBM ink. This can be due to the higher droplet spread upon impacting at a higher speed on the receiving surface.

It is possible to conclude that the sequential IJP deposition of inks for the fabrication of pseudo-PHJs leads to an efficient film interfacial mixing at lengths comparable to the thickness of the single printed layer, in turn facilitating the photogenerated exciton dissociation to free charges. A schematic representation of the complex processes occurring in the investigated systems is provided in Figure 6. In contrast to layers printed by orthogonal solvents, for which the extent of possible intermixing is low or almost negligible, a partial dissolution can be leveraged by using sets of nonorthogonal or partially miscible solvents that lead to not negligible interfacial mixing. Such interfacial mixing likely results in a suitable nanomorphology for efficient charge generation and extraction, due to the interdiffusion of the PCBM particles into the printed layer of P3HT film. The presence of PCBM aggregates at the droplet border is a direct consequence of chlorobenzene accumulation. The aggregates observed at the droplet border might, in principle, affect the morphology of the active area. Nevertheless, the judicious choice of the solvent physicochemical parameters shown in our work (i.e., combining a high surface tension less volatile solvent with lower surface tension more volatile solvent) allows confining the outcome of the Marangoni flows only at the droplet border and not on the whole intermixed area.

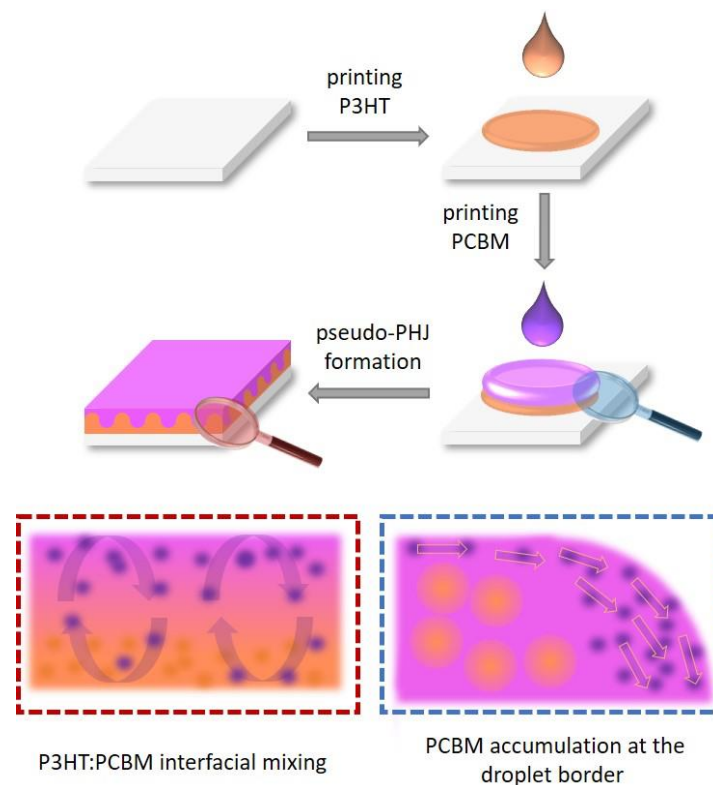


Figure 6. The interplay of interfacial mixing and Marangoni flows in sequentially printed quasi-miscible droplets. The sequential printing of quasi-miscible droplets leads to interfacial mixing of the PCBM molecules to obtain a quasi-complete mixing with the P3HT-printed layer at microsecond time scales. PCBM molecules are accumulated at the droplet border due to the chlorobenzene-driven Marangoni flows.

5. Conclusions

This study elucidates the intermixing mechanism of sequentially inkjet-printed interfaces, focusing on the model P3HT:PCBM D:A couple produced under the employ of bisolvent inks, suitable for the fabrication of OSCs. The amount of dissolution of the PHJs interface strictly depends on the physicochemical phenomena occurring in these systems, based on the interplay between evaporation and Marangoni flows. The formulated PCBM printable bisolvent ink triggers PCBM recirculation at the interface with the P3HT layer. In accordance with the models for bisolvent microdroplets, the high boiling and high surface tension chlorobenzene solvent produce a Marangoni instability at the droplet border, leading to the formation of nanoscopic aggregates. On the other hand, the center of the droplet is not affected by such instability, leading to a highly uniform surface morphology in which a consistent intermixing between the printed materials occurs, as demonstrated by the XPS depth profiles. The resulting thin-film morphology and molecular organization at the P3HT/PCBM interface were investigated by AFM, highlighting the roles of dissolution-driven molecular recirculation. This study represents a first step toward the sequential inkjet printing fabrication of pseudo-PHJs organic solar cells at low consumption of solvents/chemicals and good performances. It can also be a first step toward the engineering of a novel class of PHJs and, in general, reconfigurable mixing interfaces. In perspective, more thorough control of the molecular inks' physicochemical parameters (concentration, viscosity, and surface tension), along with the solvent boiling point and the droplet dynamics formation and impact, can be tuned to control the thickness of intermixing layers finely, opening the way to the optimization of photovoltaic devices performances while minimizing losses due to excitonic recombination. The pseudo-PHJ engineered by IJP could then be a convenient alternative with respect to PHJs or BHJs.

Supplementary Materials: The following are available online at <https://www.mdpi.com/article/10.3390/coatings11050586/s1>, Table S1: Solvents used for printing solar cells, Figure S1: Derby plot of inks used for solar cells fabrication, Figure S2: PEDOT:PSS ink deposition, Figure S3: AFM characterization of the P3HT layer printed at 40 V, Figure S4: AFM characterization of the border of the P3HT layer, Table S2: Reproducibility evaluation of the photovoltaics parameters.

Author Contributions: Conceptualization, G.A. and C.S.; methodology, C.S. and A.-G.G.; validation, C.S.; formal analysis, C.S. and M.S.; investigation, A.-G.G., S.C., M.S.; resources, B.P.; writing—original draft preparation, G.A.; writing—review and editing, A.B., G.G., and G.A.; supervision, B.P. All authors have read and agreed to the published version of the manuscript.

Funding: The Italian Ministry of University and Research (MURST, ex-MIUR) is acknowledged for funding through the program PON 12 aree di specializzazione PNR 2015-2020 (project “BEST4U Tecnologia per celle solari bifacciali ad alta efficienza a 4 terminali per utility scale”, CUP B61B19000160005). MiUR is also acknowledged for funding through the program PON “AIM: Attrazione e Mobilità Internazionale”, call AIM1809078-2 and CUP B78D19000280001. The Advanced Technologies Network (ATeN) Center (University of Palermo; project “Mediterranean Center for Human Health Advanced Biotechnologies (CHAB)”, PON R&C 2007–2013) is also acknowledged for hospitality and service.

Institutional Review Board Statement: Not applicable.

Informed Consent Statement: Not applicable.

Data Availability Statement: Data sharing is not applicable to this article.

Acknowledgments: ATeN Center (University of Palermo; project “Mediterranean Center for Human Health Advanced Biotechnologies (CHAB)”, PON R&C 2007–2013) is acknowledged for hospitality and service.

Conflicts of Interest: The authors declare no conflict of interest.

References

1. Carpenter, A. Oil pollution in the north sea: The impact of governance measures on oil pollution over several decades. *Hydrobiologia* **2019**, *845*, 109–127. [[CrossRef](#)]
2. Ahmadi, F.; Samlali, K.; Vo, P.Q.N.; Shih, S.C.C. An integrated droplet-digital microfluidic system for on-demand droplet creation, mixing, incubation, and sorting. *Lab Chip* **2019**, *19*, 524–535. [[CrossRef](#)] [[PubMed](#)]
3. Kaminski, T.S.; Garstecki, P. Controlled droplet microfluidic systems for multistep chemical and biological assays. *Chem. Soc. Rev.* **2017**, *46*, 6210–6226. [[CrossRef](#)] [[PubMed](#)]
4. Fortelný, I.; Jůza, J. Description of the droplet size evolution in flowing immiscible polymer blends. *Polymers* **2019**, *11*, 761. [[CrossRef](#)] [[PubMed](#)]
5. Goodarzi, F.; Zendehboudi, S. A comprehensive review on emulsions and emulsion stability in chemical and energy industries. *Can. J. Chem. Eng.* **2019**, *97*, 281–309. [[CrossRef](#)]
6. Ai, Y.; Xie, R.; Xiong, J.; Liang, Q. Microfluidics for biosynthesizing: From droplets and vesicles to artificial cells. *Small* **2019**, *19*, 1903940, 1–24. [[CrossRef](#)] [[PubMed](#)]
7. Arrabito, G.; Ferrara, V.; Bonasera, A.; Pignataro, B. Artificial biosystems by printing biology. *Small* **2020**, *16*, 1907691. [[CrossRef](#)] [[PubMed](#)]
8. Mouhamad, Y.; Mokarian-Tabari, P.; Clarke, N.; Jones, R.A.L.; Geoghegan, M. Dynamics of polymer film formation during spin coating. *J. Appl. Phys.* **2014**, *116*, 123513. [[CrossRef](#)]
9. Yang, H.; Jiang, P. Large-scale colloidal self-assembly by doctor blade coating. *Langmuir* **2010**, *26*, 13173–13182. [[CrossRef](#)] [[PubMed](#)]
10. Jagadamma, L.K.; Al-Senani, M.; El-Labban, A.; Gereige, I.; Ngongang Ndjawa, G.O.; Faria, J.C.D.; Kim, T.; Zhao, K.; Cruciani, F.; Anjum, D.H.; et al. Polymer solar cells with efficiency >10% enabled via a facile solution-processed Al-doped ZnO electron transporting layer. *Adv. Energy Mater.* **2015**, *5*, 1500204. [[CrossRef](#)]
11. Arrabito, G.; Cavaleri, F.; Montalbano, V.V.; Vetri, V.; Leone, M.; Pignataro, B. Monitoring few molecular binding events in scalable confined aqueous compartments by raster image correlation spectroscopy (CADRICS). *Lab Chip* **2016**, *16*, 4666–4676. [[CrossRef](#)] [[PubMed](#)]
12. Arrabito, G.; Pignataro, B. Solution processed micro- and nano-bioarrays for multiplexed biosensing. *Anal. Chem.* **2012**, *84*, 5450–5462. [[CrossRef](#)] [[PubMed](#)]
13. Miccichè, C.; Arrabito, G.; Amato, F.; Buscarino, G.; Agnello, S.; Pignataro, B. Inkjet printing Ag nanoparticles for SERS hot spots. *Anal. Methods* **2018**, *10*, 3215–3223. [[CrossRef](#)]
14. Singh, B.M.; Haverinen, H.M.; Dhagat, P.; Jabbour, G.E. Inkjet printing-process and its applications. *Adv. Mater.* **2010**, *22*, 673–685. [[CrossRef](#)] [[PubMed](#)]

15. Alamán, J.; Alicante, R.; Peña, J.I.; Sánchez-Somolinos, C. Inkjet printing of functional materials for optical and photonic applications. *Materials* **2016**, *9*, 910. [[CrossRef](#)] [[PubMed](#)]
16. Kim, D.-O.; Rokoni, A.; Kaneelil, P.; Cui, C.; Han, L.-H.; Sun, Y. Role of surfactant in evaporation and deposition of bisolvent biopolymer droplets. *Langmuir* **2019**, *35*, 12773–12781. [[CrossRef](#)] [[PubMed](#)]
17. Sowade, E.; Ramon, E.; Mitra, K.Y.; Martínez-Domingo, C.; Pedró, M.; Pallarès, J.; Loffredo, F.; Villani, F.; Gomes, H.L.; Terés, L.; et al. All-inkjet-printed thin-film transistors: Manufacturing process reliability by root cause analysis. *Sci. Rep.* **2016**, *6*, 33490. [[CrossRef](#)]
18. Grubb, P.M.; Subbaraman, H.; Park, S.; Akinwande, D.; Chen, R.T. Inkjet printing of high performance transistors with micron order chemically set gaps. *Sci. Rep.* **2017**, *7*, 1202. [[CrossRef](#)]
19. Seol, M.-L.; Han, J.-W.; Moon, D.-I.; Yoon, K.J.; Hwang, C.S.; Meyyappan, M. All-printed triboelectric nanogenerator. *Nano Energy* **2018**, *44*, 82–88. [[CrossRef](#)]
20. Saha, M.S.; Malevich, D.; Halliop, E.; Pharoah, J.G.; Peppley, B.A.; Karan, K. Electrochemical activity and catalyst utilization of low Pt and thickness controlled membrane electrode assemblies. *J. Electrochem. Soc.* **2011**, *158*, B562–B567. [[CrossRef](#)]
21. Shukla, S.; Domican, K.; Karan, K.; Bhattacharjee, S.; Secanell, M. Analysis of low platinum loading thin polymer electrolyte fuel cell electrodes prepared by inkjet printing. *Electrochim. Acta* **2014**, *156*, 289–300. [[CrossRef](#)]
22. Yeh, N.; Yeh, P. Organic solar cells: Their developments and potentials. *Renew. Sustain. Energy Rev.* **2013**, *21*, 421–431. [[CrossRef](#)]
23. Lange, A.; Wegener, M.; Fischer, B.; Janietz, S.; Wedel, A. Solar cells with inkjet printed polymer layers. *Energy Procedia* **2013**, *31*, 150–158. [[CrossRef](#)]
24. Teichler, A.; Eckardt, R.; Hoepfener, S.; Friebe, C.; Perelaer, J.; Senes, A.; Morana, M.; Brabec, C.J.; Schubert, U.S. Combinatorial screening of polymer: Fullerene blends for organic solar cells by inkjet printing. *Adv. Energy Mater.* **2011**, *1*, 105–114. [[CrossRef](#)]
25. Eom, S.H.; Senthilarasu, S.; Uthirakumar, P.; Yoon, S.C.; Lim, J.; Lee, C.; Lim, H.S.; Lee, J.; Lee, S.H. Polymer solar cells based on inkjet-printed PEDOT:PSS layer. *Org. Electron.* **2009**, *10*, 536–542. [[CrossRef](#)]
26. Jung, S.; Sou, A.; Banger, K.; Ko, D.H.; Chow, P.C.Y.; McNeill, C.R.; Siringhaus, H. All-inkjet-printed, all-air-processed solar cells. *Adv. Energy Mater.* **2014**, *4*, 1–9. [[CrossRef](#)]
27. Abulikemu, M.; Da'as, E.H.; Haverinen, H.; Cha, D.; Malik, M.A.; Jabbour, G.E. In situ synthesis of self-assembled gold nanoparticles on glass or silicon substrates through reactive inkjet printing. *Angew. Chem.* **2014**, *126*, 430–433. [[CrossRef](#)]
28. Teo, M.Y.; Stuart, L.; Aw, K.C.; Stringer, J. Micro-reactive inkjet printer for 2D and 3D hydrogel structures. In Proceedings of the 2018 IEEE/ASME International Conference on Advanced Intelligent Mechatronics (AIM), Auckland, New Zealand, 9–12 July 2018; pp. 569–573. [[CrossRef](#)]
29. Wei, Z.; Li, Y.; Cooks, R.G.; Yan, X. Accelerated reaction kinetics in microdroplets: Overview and recent developments. *Annu. Rev. Phys. Chem.* **2020**, *71*, 31–51. [[CrossRef](#)] [[PubMed](#)]
30. Peng, X.; Yuan, J.; Shen, S.; Gao, M.; Chesman, A.S.R.; Yin, H. Perovskite and organic solar cells fabricated by inkjet printing: Progress and prospects. *Adv. Funct. Mater.* **2017**, *27*, 1703704. [[CrossRef](#)]
31. Karunakaran, S.K.; Arumugam, G.M.; Yang, W.; Ge, S.; Khan, S.N.; Lin, X.; Yang, G. Recent progress in inkjet-printed solar cells. *J. Mater. Chem. A* **2019**, *7*, 13873–13902. [[CrossRef](#)]
32. Bonasera, A.; Giuliano, G.; Arrabito, G.; Pignataro, B. Tackling performance challenges in organic photovoltaics: An overview about compatibilizers. *Molecules* **2020**, *25*, 2200. [[CrossRef](#)] [[PubMed](#)]
33. Syu, Y.-W.; Huang, P.-Y.; Li, H.-D.; Hsu, C.-L.; Chiu, K.-C.; Kim, C.; Chen, M.-C.; Chao, Y.-C. Enhanced performance of pseudo-bilayer organic photovoltaic devices via small molecule doping. *J. Phys. Chem. C* **2014**, *118*, 9958–9965. [[CrossRef](#)]
34. Lee, J.; Jung, Y.K.; Lee, D.Y.; Jang, J.-W.; Cho, S.; Son, S.; Jeong, J.; Park, S.H. Enhanced efficiency of bilayer polymer solar cells by the solvent treatment method. *Synth. Met.* **2015**, *199*, 408–412. [[CrossRef](#)]
35. Tada, A.; Geng, Y.; Wei, Q.; Hashimoto, K.; Tajima, K. Tailoring organic heterojunction interfaces in bilayer polymer photovoltaic devices. *Nat. Mater.* **2011**, *10*, 450. [[CrossRef](#)] [[PubMed](#)]
36. Kitchen, B.; Awartani, O.; Kline, R.J.; McAfee, T.; Ade, H.; O'Connor, B.T. Tuning open-circuit voltage in organic solar cells with molecular orientation. *ACS Appl. Mater. Interfaces* **2015**, *7*, 13208–13216. [[CrossRef](#)] [[PubMed](#)]
37. Huang, L.; Jiang, P.; Zhang, Y.; Zhang, L.; Yu, Z.; He, Q.; Zhou, W.; Tan, L.; Chen, Y. Unraveling the morphology in solution-processed pseudo-bilayer planar heterojunction organic solar cells. *ACS Appl. Mater. Interfaces* **2019**, *11*, 26213–26221. [[CrossRef](#)]
38. Sartorio, C.; Scaramuzza, S.; Cataldo, S.; Vetri, V.; Scopelliti, M.; Leone, M.; Amendola, V.; Pignataro, B.; Scienze, V.; Li, O. Donor–acceptor interfaces by engineered nanoparticles assemblies for enhanced efficiency in plastic planar heterojunction solar cells. *J. Phys. Chem. C* **2016**, *120*, 26588–26599. [[CrossRef](#)]
39. Wan, J.; Zhang, L.; He, Q.; Liu, S.; Huang, B.; Hu, L.; Zhou, W.; Chen, Y. High-performance pseudoplanar heterojunction ternary organic solar cells with nonfullerene alloyed acceptor. *Adv. Funct. Mater.* **2020**, *30*, 1–9. [[CrossRef](#)]
40. Shan, T.; Hong, Y.; Zhu, L.; Wang, X.; Zhang, Y.; Ding, K.; Liu, F.; Chen, C.C.; Zhong, H. Achieving optimal bulk heterojunction in all-polymer solar cells by sequential processing with nonorthogonal solvents. *ACS Appl. Mater. Interfaces* **2019**, *11*, 42438–42446. [[CrossRef](#)] [[PubMed](#)]
41. Zhang, X.; Öberg, V.A.; Du, J.; Liu, J.; Johansson, E.M.J. Extremely lightweight and ultra-flexible infrared light-converting quantum dot solar cells with high power-per-weight output using a solution-processed bending durable silver nanowire-based electrode. *Energy Environ. Sci.* **2018**, *11*, 354–364. [[CrossRef](#)]

42. Carlé, J.E.; Helgesen, M.; Hagemann, O.; Hösel, M.; Heckler, I.M.; Bundgaard, E.; Gevorgyan, S.A.; Søndergaard, R.R.; Jørgensen, M.; García-Valverde, R.; et al. Overcoming the scaling lag for polymer solar cells. *Joule* **2017**, *1*, 274–289. [[CrossRef](#)]
43. Li, Y.; Xu, G.; Cui, C.; Li, Y. Flexible and semitransparent organic solar cells. *Adv. Energy Mater.* **2018**, *8*, 1701791. [[CrossRef](#)]
44. Schubert, M.B.; Werner, J.H. Flexible solar cells for clothing. *Mater. Today* **2006**, *9*, 42–50. [[CrossRef](#)]
45. Hashemi, S.A.; Ramakrishna, S.; Aberle, A.G. Recent progress in flexible–wearable solar cells for self-powered electronic devices. *Energy Environ. Sci.* **2020**, *13*, 685–743. [[CrossRef](#)]
46. Nečas, D.; Klapeček, P. Gwyddion: An open-source software for spm data analysis. *Cent. Eur. J. Phys.* **2012**, *10*, 181–188. [[CrossRef](#)]
47. Srivastava, R.; Natarajan, G.; Smith, B.D. Total pressure vapor-liquid equilibrium data for binary systems of diethylether with acetone, acetonitrile, and methanol. *J. Chem. Eng. Data* **1986**, *31*, 89–93. [[CrossRef](#)]
48. Srivastava, R.; Smith, B.D. Total pressure vapor-liquid equilibrium data for binary systems of dichloromethane with benzene, toluene, nitromethane, and chlorobenzene. *J. Chem. Eng. Data* **1985**, *30*, 313–318. [[CrossRef](#)]
49. Dong, H.; Carr, W.W.; Morris, J.F. An experimental study of drop-on-demand drop formation. *Phys. Fluids* **2006**, *18*, 072102. [[CrossRef](#)]
50. Sartorio, C.; Giuliano, G.; Scopelliti, M.; Vetri, V.; Leone, M.; Pignataro, B. Synergies and compromises between charge and energy transfers in three-component organic solar cells. *Phys. Chem. Chem. Phys.* **2020**, *22*, 8344–8352. [[CrossRef](#)] [[PubMed](#)]
51. Kadem, B.Y.; Al-Hashimi, M.K.; Hassan, A.K. The effect of solution processing on the power conversion efficiency of P3HT-based organic solar cells. *Energy Procedia* **2014**, *50*, 237–245. [[CrossRef](#)]
52. Sartorio, C.; Campisciano, V.; Chiappara, C.; Cataldo, S.; Scopelliti, M.; Gruttadauria, M.; Giacalone, F.; Pignataro, B. Enhanced power-conversion efficiency in organic solar cells incorporating copolymeric phase-separation modulators. *J. Mater. Chem. A* **2018**, *6*, 3884–3894. [[CrossRef](#)]
53. Burgués-Ceballos, I.; Hermerschmidt, F.; Akkuratov, A.V.; Susarova, D.K.; Troshin, P.A.; Choulis, S.A. High-performing poly-carbazole derivatives for efficient solution-processing of organic solar cells in air. *Chemsuschem* **2015**, *8*, 4209–4215. [[CrossRef](#)] [[PubMed](#)]
54. Hu, H.; Larson, R.G. Evaporation of a sessile droplet on a substrate. *J. Phys. Chem. B* **2002**, *106*, 1334–1344. [[CrossRef](#)]
55. Belmiloud, N.; Tamaddon, A.H.; Mertens, P.W.; Struyf, H.; Xu, X. Dynamics of the drying defects left by residual ultra-pure water droplets on silicon substrate. *ECS J. Solid State Sci. Technol.* **2012**, *1*, 34–39. [[CrossRef](#)]
56. Hattori, Y.; Haruna, Y.; Otsuka, M. Dissolution process analysis using model-free noyes-whitney integral equation. *Colloids Surf. B* **2013**, *102*, 227–231. [[CrossRef](#)] [[PubMed](#)]
57. Treat, N.D.; Mates, T.E.; Hawker, C.J.; Kramer, E.J.; Chabynyc, M.L. Temperature dependence of the diffusion coefficient of PCBM in poly(3-hexylthiophene). *Macromolecules* **2013**, *46*, 1002–1007. [[CrossRef](#)]
58. Machui, F.; Langner, S.; Zhu, X.; Abbott, S.; Brabec, C.J. Determination of the P3HT:PCBM solubility parameters via a binary solvent gradient method: Impact of solubility on the photovoltaic performance. *Sol. Energy Mater. Sol. Cells* **2012**, *100*, 138–146. [[CrossRef](#)]
59. Deegan, R.D.; Bakajin, O.; Dupont, T.F.; Huber, G.; Nagel, S.R.; Witten, T.A. Capillary flow as the cause of ring stains from dried liquid drops. *Nature* **1997**, *389*, 827. [[CrossRef](#)]
60. Eales, A.D.; Dartnell, N.; Goddard, S.; Routh, A.F. Thin, binary liquid droplets, containing polymer: An investigation of the parameters controlling film shape. *J. Fluid Mech.* **2016**, *794*, 200–232. [[CrossRef](#)]
61. Suri, S.K.; Ramakrishna, V. Surface tension of some binary liquid mixtures. *J. Phys. Chem.* **1968**, *72*, 3073–3079. [[CrossRef](#)]